2012-2-1

Temperature Dependence of the Infrared Absorption Cross-Sections of Neutral Species Commonly Found in Fluorocarbon Plasmas

Caleb T. Nelson, *et al.*

JVSTA
JOURNAL OF VACUUM SCIENCE AND TECHNOLOGY A

Temperature dependence of the infrared absorption cross-sections of neutral species commonly found in fluorocarbon plasmas

Caleb T. Nelson, Lawrence J. Overzet, and Matthew J. Goeckner

Citation: J. Vac. Sci. Technol. A **30**, 021305 (2012); doi: 10.1116/1.3679408
View online: http://dx.doi.org/10.1116/1.3679408
View Table of Contents: http://avspublications.org/resource/1/JVTAD6/v30/i2
Published by the AVS: Science & Technology of Materials, Interfaces, and Processing

Temperature dependence of the infrared absorption cross-sections of neutral species commonly found in fluorocarbon plasmas

Caleb T. Nelson, Lawrence J. Overzet,[a] and Matthew J. Goeckner[a]
Department of Electrical Engineering, University of Texas at Dallas, P.O. Box 830688, Richardson, Texas 75083

(Received 5 April 2011; accepted 19 December 2011; published 1 February 2012)

This article serves as a reference for the analysis of Fourier transform infrared spectroscopy data from processing plasmas. Until now, there has been a lack of accurate reference data for addressing the problems of species identification and density measurements in cases of increasing gas temperatures. Our results show that, while the integrated absorption cross-sections do not change significantly as temperature increases, the temperature of the absorbing species can be estimated from the rotational band maximum in most cases. Integrated absorption cross-sections for *c*-C_3F_6, C_4F_8, C_3F_8, C_2F_6, C_2F_4, and CF_4 are presented for all fundamental bands in the 650 cm^{-1} to 2000 cm^{-1} region. In addition, the binary combination bands up to 4000 cm^{-1} are presented for all species. The temperature of each species has been varied to correspond to neutral temperatures commonly found in processing plasmas. © *2012 American Vacuum Society*. [DOI: 10.1116/1.3679408]

I. INTRODUCTION

Fourier transform infrared spectroscopy (FTIR) has been widely used in chemistry research since the 1960s.[1] The efficiency of information gathering and the affordability of this diagnostic tool have allowed it to become the predominant method for obtaining infrared spectra of chemistries in all states of matter. More recently, *in situ* FTIR has begun to be used as a gas-phase diagnostic tool in studying plasma processes.[2,3] This technique allows several advantages over optical emission measurements, laser induced fluorescence (LIF), and infrared laser absorption spectroscopy (LAS).[4] It is a nonintrusive technique and offers the advantage of broadband absorption, allowing the detection of multiple species simultaneously, including unanticipated species that might be present in the system. Such simultaneous detection of species, both anticipated and unanticipated, including higher mass species, is difficult with either LIF or LAS. However, with this technique it is difficult to accurately identify the source of unanticipated infrared absorption. This problem is exacerbated in Fourier transform IR spectroscopy because of the multitude of species (which often have overlapping absorption bands) present within plasmas. This dilemma has been approached through modeling with commercial programs such as SPARTAN© and GAUSSIAN©,[5] as well as through limited experimental measurements. Commercial modeling suffers from unknowns and approximations; however, experimental measurements often include insufficient temperature control of the radical being measured, problems associated with gas contamination, and instrumental variations.

While some researchers have addressed gas temperature-related absorption variations for atmospheric gases in the range of 198 to 273 K,[6,7] very few papers examine temperature-induced effects on the structure and absorption cross-sections of plasma processing gases, which often operate well above room temperature. The only currently used fluorocarbon that has been analyzed for temperature measurement is CF_4.[8] Knowing how absorption spectra change with varying temperatures is particularly important when using FTIR as an *in situ* technique for accurately predicting the consumption of the parent feed gas and the steady-state densities of by-products present within the plasma. This is because of the gas temperature changes inherent in an excited system.

A number of researchers, including the authors of this article, have used *in situ* FTIR to understand fluorocarbon plasmas over the past decade.[9–14] However, due to the lack of literature available, there has been difficulty accurately identifying species within the absorption spectra, as well as translating absorption areas to absolute densities for those species already identified.

It is the purpose of this paper to provide reference data for use in understanding FTIR results from fluorocarbon plasmas. The use of infrared absorption both as a means of partial pressure measurement and gas temperature measurement will be discussed. A brief experimental setup and a discussion of theoretical gas temperature effects on infrared absorption will be given before providing relevant results and conclusions.

II. EXPERIMENTAL SETUP

Spectral data was taken by a Nicolet 870 Fourier-transform spectrometer. A globar source and a KBr beam splitter were used to measure a spectrum from 4000 cm^{-1} to 650 cm^{-1}. A diagram of the FTIR bench and the chamber is supplied in Fig. 1. The path length of the chamber (81.25 cm) was extended by installing a custom fit Gemini® White cell. This allowed the path length to be varied from 3.25 m (4 pass) to 19.5 m (24 pass), providing the ability to observe bands with small cross-sections at low pressures. The mirrors of the White cell were gold-plated in order to reduce IR losses on each reflection (<5%). The IR beam entered and exited the chamber through 4 mm KBr windows. An additional KBr window (6 mm) was installed on the FTIR bench. The signal was collected by a cryogenically cooled Mercury-cadmium-telluride (MCT-A) detector. Mirror velocity was set to 4.7468 cm/s and 64 scans were averaged at 0.125 cm^{-1} resolution. A Happ-Genzel apodization and a Mertz phase correction were applied to the final spectrum.

[a]Author to whom correspondence should be addressed; electronic mail: goeckner@utdallas.edu

Gases were purchased from a variety of sources. Specialty Gases of America supplied 99.9% pure octafluorocylobutane (C_4F_8), perfluoropropane (C_3F_8), and hexafluoropropylene (C_3F_6). Matheson Tri-Gas provided 99.99% pure tetrafluoromethane (CF_4) and 99% pure tetrafluoroethylene (C_2F_4). These gases were continuously flowed into a 100 L reactor chamber, which was pressure-controlled to $\pm 1 \times 10^{-4}$ Torr by a MeiVac throttle valve through a feedback loop to a MKS 252 A exhaust valve controller. An Osaka Vacuum compound molecular pump provided a base pressure of 1×10^{-6} Torr. More information about the vacuum reactor design is included elsewhere.[15] Pressure variations across the chamber were minimized by ensuring that the diffusion time to the walls was much less than the residence time in the chamber. For the conditions considered, this ratio was maintained at a minimum of 25 by limiting the gas flow rate to 10 sccm. Finally, the pressure measurements were validated by comparing calculated cross-sections to those available in literature. Inside the 66 cm diameter cylindrical reactor, a 60 cm diameter temperature-controlled aluminum wall was used to vary the temperature from 25 °C to 225 °C. These walls were complemented by temperature-controlled floor and ceiling plates, located 2 cm from the vertical ports of the chamber. Temperature was measured using a combination of six K-type and T-type thermocouples controlled through an Omega CN616 multizone temperature controller. The accuracy of the local temperature measurements is within 1 °C. However, due to the large wall area, local temperatures varied by up to 3 °C. Prior to each experiment, the temperature was allowed to stabilize for 2 hs in order to avoid changes in temperature during the course of the experiment. The gas temperatures used for density calculations were taken by assuming a linear change in temperature from the inner wall (60 cm diameter) to the outer wall (66 cm diameter) of the chamber. The reported temperature is averaged across the infrared beam path, the majority of which (>80%) lies within the heated walls (see Fig. 1). Additionally, the outer walls equilibrated to the mean between the room temperature and the inner chamber temperature, further minimizing temperature variations across the system. The validity of the temperature measurement across the system can be verified by the fact that the integrated absorption cross-sections across measured gases do not change significantly (<5%) with temperature. Spectra were collected for each gas at temperatures of 25, 50, 100, 150, and 200 °C.

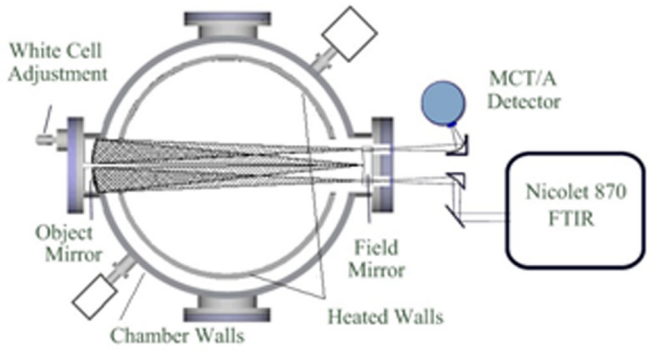

FIG. 1. (Color online) Experimental setup showing the FTIR bench and White cell.

III. DENSITY ESTIMATION FROM INFRARED ABSORBANCE

Absorption cross-sections were obtained from measured signal intensities according to Beer's Law,[16]

$$A(\lambda) = -\ln\left(\frac{I(\lambda)}{I_0(\lambda)}\right) = nl\sigma(\lambda), \quad (1)$$

$$I(\lambda) = I_0(\lambda)e^{-nl\sigma(\lambda)}, \quad (2)$$

where $\sigma(\lambda)$ is the absorption cross-section at wavelength λ in cm^2 $molecule^{-1}$, I_0 and I are incident and transmitted radiation, n is the concentration of the gas being measured in cm^{-3}, and l is the path length of the sample in cm. The natural log definition of absorbance is used in convention with standards for gases. Beer's law predicts a linear relationship between the number of molecules in the path of the radiation and the absorbance. This holds true in all cases where the absorbers act independently from one another, the radiation is not significantly scattered by the absorbing medium, and there is neither optical pumping of the species being observed nor saturation of the impinging radiation. For all gases except CF_4, the absorption was observed to increase linearly with pressure and path length, validating the relationship in Eq. (1).

Once the absorption cross-section has been determined, species densities can be determined from the measured absorption spectra via Eq. (1). When calculating absolute densities using integrated absorbance cross-sections, it is important to consider error due to underlying absorption from other species. In order to reduce this error, the absorbance of multiple normal modes can be used. The standard deviation of the calculated densities for a species can reveal any unanticipated underlying absorption, allowing for increased accuracy in density measurements.

IV. TEMPERATURE ESTIMATION FROM INFRARED ABSORBANCE

A variety of methods have been used to estimate temperature from the intensity distribution in infrared vibrational-rotational bands. However, resolution limitations restrict some of these methods. The intersection of two branches shifts to higher rotational states as temperature increases. Although this method has been used to measure the temperature of carbon monoxide,[17] it is not useful for most band shapes. Another method uses the shape of the band profile to determine temperature.[18,19] While this method is useful for interpreting the temperature from the absorption of isolated species, the simultaneous absorption of many gaseous species at identical or adjacent wavenumbers creates overlapping band structures, which are difficult to deconvolve.

The location of a branch maximum can also be used to estimate the gas rotational temperature. This method can provide an approximation even when the band structures are overlapping as long as the branch maxima are sufficiently separated to observe the shift with temperature. For the simplified case where a diatomic molecule is modeled as a rigid rotor, Eq. (3) describes how the number of molecules in a specific rotational state changes with temperature.

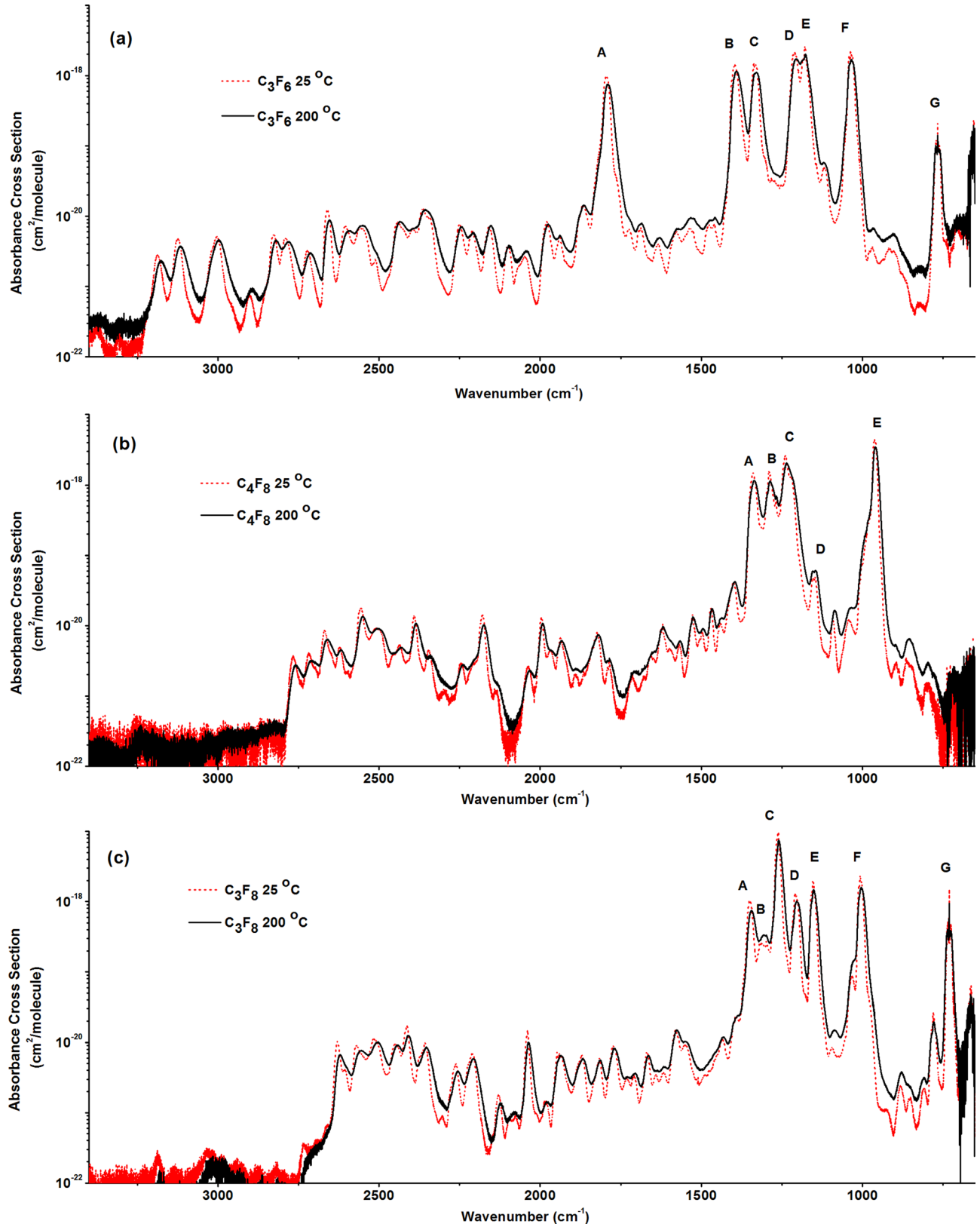

FIG. 2. (Color online) Absorption cross-section from 400 to 4000 cm^{-1} wavenumbers on a semilog scale for 25 and 200 °C gas temperatures. Absorption cross-sections are created from a compilation of the infrared absorption of pure gases at various pressures (0.001 – 1 Torr) and pathlengths (3.25 – 19.5 m). (a) C_3F_6, (b) C_4F_8, (c) C_3F_8. Band designations appearing in the figure are provided in Tables I, II, and III, respectively.

$$N_J \propto (2J+1)e^{-\frac{BJ(J-1)hc}{kT}}. \quad (3)$$

Setting the slope of this curve to zero leads to the rotational state with the maximum number of molecules J_{max}. J_{max} increases with the square root of temperature, as seen in Eq. (4) of Ref. 20.

$$J_{max} = \sqrt{\frac{kT}{2Bhc}} - \frac{1}{2}. \quad (4)$$

In these equations, T is the temperature of the species in Kelvin, h is Planck's constant, c is the speed of light, and B is the rotational constant. The wavenumber spacing of the rotational levels can be approximated by treating the vibration as a harmonic oscillator. Under this assumption, the wavenumber for a transition between rotational states J' and $J''$is described by Eq. (5) of Ref. 20.

$$\upsilon = \upsilon_0 + B'J'(J'+1) - B''J''(J''+1). \quad (5)$$

Here, υ_0 is the frequency of the vibrational transition at $J' = J'' = 0$, B' and B'' are the rotational constants and J' and J'' are the rotational states. If only the ground vibrational state is populated and the interaction between rotation and vibration is neglected, this equation can be reduced to a set of equations for $J' - J'' \equiv \Delta J \pm 1$ where $B' = B''$:[20]

$$\Delta J = +1 \rightarrow \upsilon = \upsilon_0 + 2B(J''+1), \quad (6)$$

$$\Delta J = -1 \rightarrow \upsilon = \upsilon_0 - 2BJ''. \quad (7)$$

Although the interaction between vibration and rotation can change this relationship, Eqs. (3)–(7) lead to a first order dependency, where the rotational state with the most molecules absorbs at a given frequency that shifts proportionally with the square root of temperature.

$$\upsilon_{max} \propto \sqrt{T}. \quad (8)$$

It is worth noting that this relationship can be complicated by a number of factors. Larger molecules can deviate from these formulations. Vibration and rotation can interact, such that the rotational states are not equally spaced. Secondly, in peaks without distinguishable P, Q, and R branches, it is possible to confuse the various branch maxima as temperature increases. Finally, the formation of hot bands in the vicinity of the branch maxima can alter the perceived location of the maxima. Despite these concerns, the experimental data presented below match the theoretical dependency within the limits of experimental error. We note that it is unreliable to extrapolate the empirical equations for temperature dependency presented here to higher temperature ranges due to the possible formation of hot bands and other distorting factors. In addition, induced noise from infrared light emitted from the plasma add to the uncertainty of peak locations.

V. RESULTS AND DISCUSSION

Observing the combination of fluorocarbon species spectra and corresponding cross-sectional shifts with temperature is necessary for accurate identification of species, the detection of average gas temperatures, and the understanding of errors involved in using integrated cross-sections to produce absolute species densities. The results will be given in order of difficulty starting with the easiest species to isolate in fluorocarbon discharges. By isolating a spectral band of an individual species, the density and internal temperature of the species can be determined. After these values have been determined, the entire spectra for that species can be subtracted from the total spectra, allowing for further identification and isolation of other species. Only C_4F_8, C_3F_8, C_3F_6, C_2F_6, C_2F_4, and CF_4 will be considered in the following analysis, as these are the major (>1%) stable neutral species observed by the authors in fluorocarbon discharges. Figures 2 and 3 show the absorbance cross-sections of each species at wavelengths of 400 to 4000 cm^{-1} for gas temperatures of 25 and 200 °C. These provide a fingerprint of most of the fundamentals, as well as binary combinations and overtones for species identification.

A. C_3F_6

The fundamental band of hexafluoropropylene (C_3F_6) shown in Fig. 4 at 1789 cm^{-1} is the easiest band to identify and isolate out of all the spectra examined. It is clearly isolated from fundamental absorption bands in other fluorocarbon spectra. The presence of this band is associated with the stretching of the carbon-carbon double bond. As seen in Figs. 2 and 3, the absorbance cross-section is approximately 200 times larger than that of any other fluorocarbon species in the spectral region. Visible fundamentals and their associated absorbance cross sections can be found in Table I.

The temperature associated with this main band of C_3F_6 can be determined according to the empirical relationship:

$$T = (-7.041\upsilon_{max} + 1281.6)^2. \quad (9)$$

Here, υ_{max} is the wavenumber of the band maxima in cm^{-1} and T is the temperature in Kelvin. Absorption spectra were taken at 298, 332, 372, 422, and 474 K for fitting the rotational maximum. Calculating the standard deviation of the residual and adding the error due to the instrumental maximum resolution (0.125 cm^{-1}) yields a total minimum error of ±10.4 K.

B. c-C_4F_8

Octafluorocyclobutane, while unlikely to form as a byproduct from smaller monomer feed gases because of its cyclic structure, is a frequently used source gas for deposition processes. As can be seen in Fig. 5, its infrared absorption is marked by a very strong rotational-vibrational band at 963 cm^{-1}, a series of overlapping fundamentals in the 1100 to 1500 cm^{-1} region, and (as seen in Fig. 2) much weaker binary and ternary combinations throughout the spectrum. There has been some discussion in literature about the assignment of the fundamental bands, focusing on the identification of the puckering structure. The most recent of these papers[21] has identified the 1220 cm^{-1} band with weak

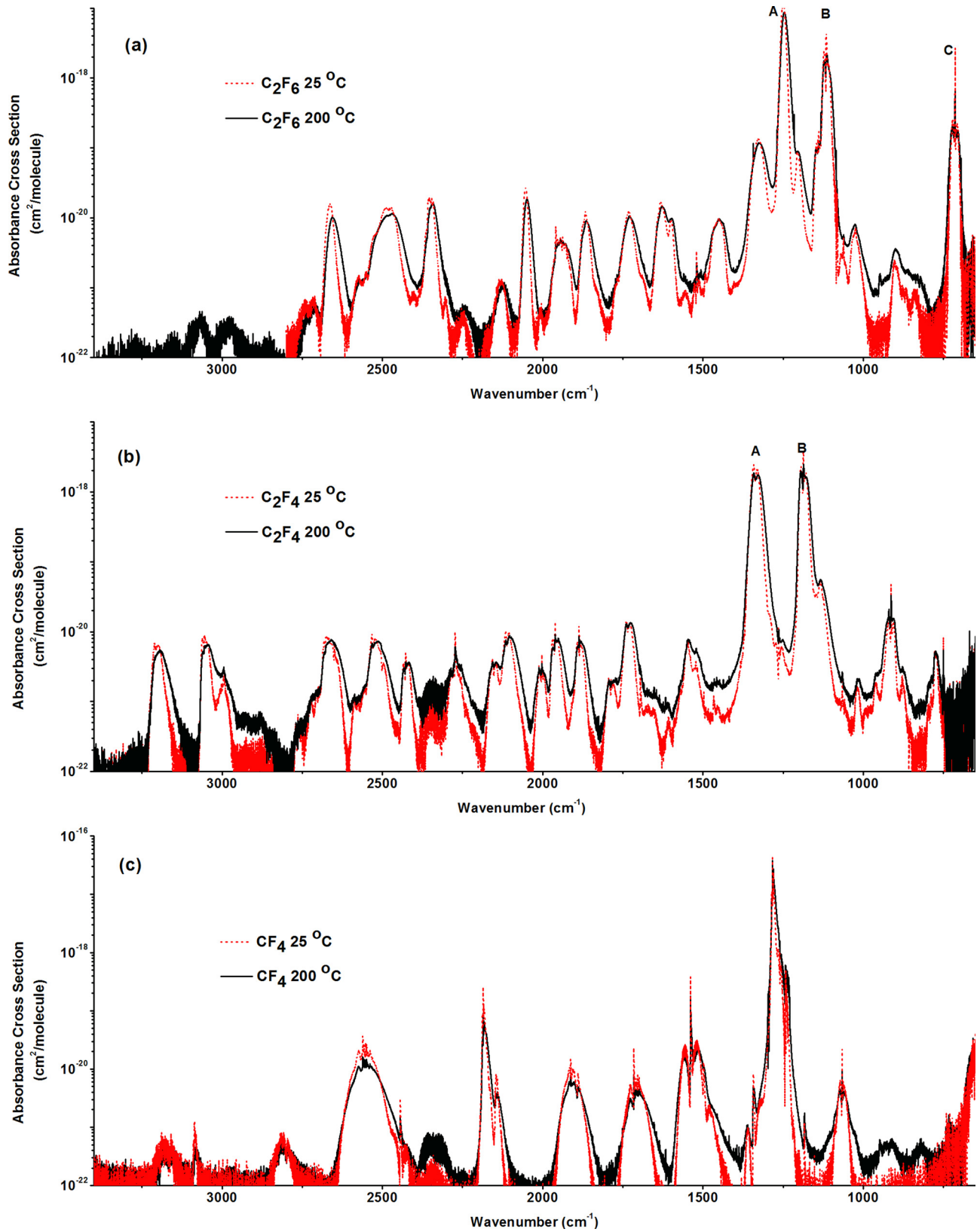

FIG. 3. (Color online) Absorption cross-section from 400 to 4000 cm^{-1} wavenumbers on a semilog scale for 25 and 200 °C gas temperatures. Absorption cross-sections are created from a compilation of the infrared absorption of pure gases at various pressures (0.001 – 1 Torr) and pathlengths (3.25 – 19.5 m). (a) C_2F_6, (b) C_2F_4, (c) CF_4. (Because of nonlinearity, CF_4 measurements were taken at 85 mTorr with a 19.5 m path length except for wavenumbers 1250–1290, which were taken at a pressure of 2 mTorr and a path length of 325 cm). Band designations appearing in the figure for C_2F_6 and C_2F_4 are provided in Tables IV and V, respectively.

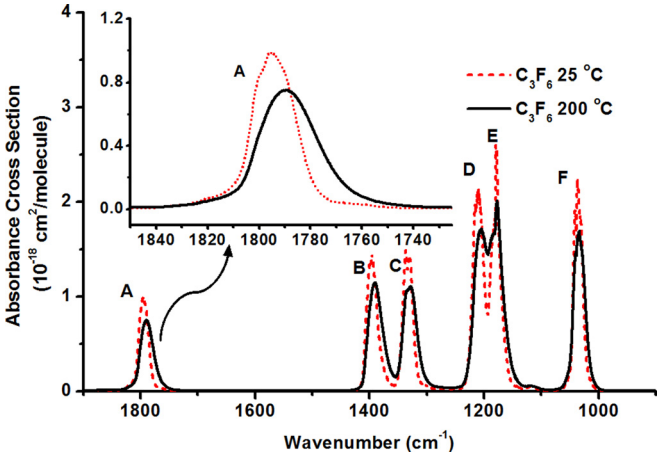

FIG. 4. (Color online) Absorbance cross-section of C_3F_6 from 900 to 1700 cm^{-1} for 25 and 200 °C gas temperatures, highlighting the C=C stretch band. Capital letter band structure designations can be found in Table I.

sidebands around 1150 cm^{-1} and 1290 cm^{-1} as evidence of the ring puckering structure of *c*-C_4F_8. Others[22] have denied the existence of an active puckering band or located it at 1340 cm^{-1}. This determination could be important in observing the existence and/or decrease of *c*-C_4F_8 in the gas. The authors of this article have been unable to locate published infrared spectra for other forms of C_4F_8. Fundamental bands and their integrated absorbance cross-sections are presented in Table II. The absorbance cross-sections are within 3% of previously published values.[23]

The C-F deformation band centered near 963 cm^{-1} provides the easiest band to isolate from other fluorocarbon gases. The absorption of perfluorobutane (C_4F_{10}) is the most significant problem in using this band for identification and measurement. A medium absorption band for perfluorobutane appears at 960 cm^{-1}.[24,25] The band is similar in shape and shifted a mere 3 cm^{-1}, allowing for confusion in identification. However, while the absorbance cross-section of C_4F_{10} is significant at 9% of the C_4F_8 cross-section, a strong band at 902 cm^{-1} can be used to identify and subtract C_4F_{10} from the spectrum.[25]. C_3F_8 also absorbs IR at 1007 cm^{-1}, allowing the tail of this band to obscure the leading edge of the C_4F_8 963 cm^{-1} band. The peak can be identified and subtracted by using the range around the peak maximum (965–950 cm^{-1}) where the absorbance cross-section is more than three orders of magnitude larger than other fluorocarbon species. Other

TABLE II. Band assignments and integrated absorption cross-sections for C_4F_8 taken at room temperature. Integrated cross-sections were also taken for 200 °C. The latter values were within 5% of those listed here.

	Band (cm^{-1})	Assignment	Range (cm^{-1})	Integrated Absorbance Cross-Section (cm/molecule)
A	1340	C-C Stretch		
B	1289	CF_2 Sym Stretch		
C	1239	CF_2 Asym Stretch-bend	1100–1500 [a]	1.438×10^{-16} [a]
D	1220	CF_2 Sym Stretch		
E	963	CF_2 Stretch-bend	900–1050	6.677×10^{-17}

[a]Bands at 1220, 1239, 1289, and 1340 cm^{-1} were combined for the cross-section provided.

fundamentals and their associated assignments and integrated absorption cross-sections can be found in Table II.

The peak maximum of the C-F deformation band at 963 cm^{-1} can also be used for a rough temperature estimate. As seen in Fig. 5, the rotational line with the maximum absorption shifts by 3 cm^{-1}. Again, applying a rough linear fit, the relationship can be modeled as:

$$T = (-1.337\upsilon_{\max} + 1305.6)^2. \quad (10)$$

Taking the standard deviation of the residual and adding the error from the instrumental resolution (0.125 cm^{-1}) gives a minimum error of ±8.2 K. Multiple band heads and/or multiple points on the 960 cm^{-1} band can be used to decrease this error slightly.

C. C_3F_8

Perfluoropropane has been used as an alternative source of fluorine for a variety of applications.[26] It is also a potential product from other fluorocarbon plasmas. The infrared spectrum includes strong absorption corresponding to C-F stretching at 1350, 1262, 1210, 1155, 1007, and 731 cm^{-1}. Tabulated in Table III, these bands, assignments,[27] and cross-sections, show good agreement with related literature.[25] As seen in Fig. 6, the CF_3 asymmetric stretching at 1007 cm^{-1} is the easiest band to use for identification and temperature measurements in a fluorocarbon mixture. Both the 1037 cm^{-1} C_3F_6 and 963 cm^{-1} C_4F_8 bands previously mentioned have a small

TABLE I. Band assignments and integrated absorption cross-sections for C_3F_6 taken at room temperature. Integrated cross-sections were also taken for 200 °C. These values were within 5% of those listed here.

	Band (cm^{-1})	Assignment	Range (cm^{-1})	Integrated Absorbance Cross-Section (cm/molecule)
A	1789	C=C Stretch	1700–1850	2.22×10^{-17}
B	1398	CF_3 sym Stretch	1355–1420	3.41×10^{-17}
C	1336	CF_2 sym Stretch	1275–1355	3.3×10^{-17}
D	1211	CF_3 asym Stretch	1100–1250[a]	9.73×10^{-17}[a]
E	1179	CF_3 asym Stretch		
F	1037	CF Stretch	975–1075	4.15×10^{-17}
G	767	C-C Stretch	740–800	2.23×10^{-18}

[a]Bands at 1211 cm^{-1} and 1179 cm^{-1} were combined for the cross-section provided.

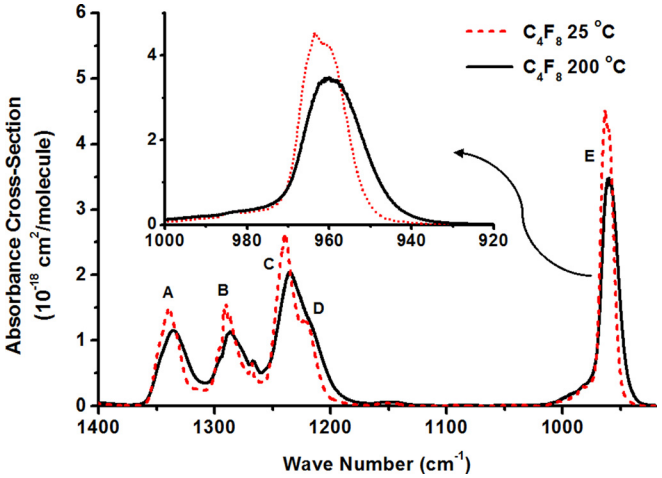

FIG. 5. (Color online) Absorbance cross-section of c-C_4F_8 from 850 to 1400 cm^{-1} for 25 and 200 °C gas temperatures, highlighting the CF_2 stretch band. Capital letter band structure designations can be found in Table II.

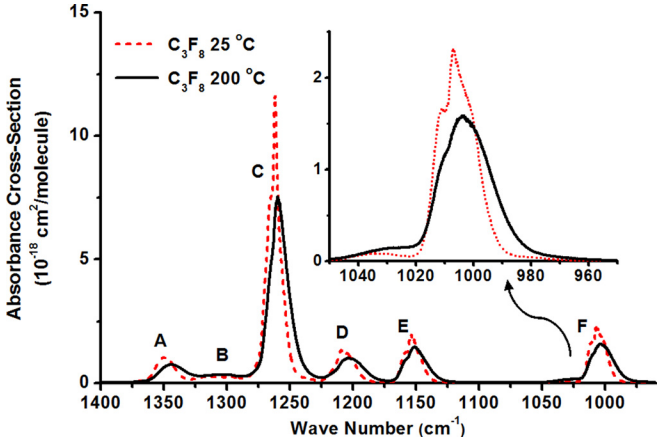

FIG. 6. (Color online) Absorbance cross-section of C_3F_8 from 950 to 1400 cm^{-1} for 25 and 200 °C gas temperatures, highlighting the C-C Asymmetric stretch band shift with temperature. Capital letter band structure designations can be found in Table III.

amount of overlapping absorbance. However, the absorbance bands of both of these species can be subtracted according to the methodology above. At the peak maximum, absorbance of C_3F_8 is 50 times larger than either C_4F_8 or C_3F_6, making it useful for both identification and temperature estimation.

The wavenumber of the peak maximum is proportional to the square root of the temperature with a R^2 value of 0.9993. The empirical relationship can be described as:

$$T = (-1.3965\upsilon_{\max} + 1423.3)^2. \quad (11)$$

Taking the sum of the standard deviation of the residual and the instrumental error leads to a minimum error of ±8.1 K.

D. C_2F_6

Hexafluoroethane (C_2F_6) is commonly used as a source gas for etching a variety of oxides.[28] It can also be formed in other fluorocarbon plasmas through electron impact dissociation of C_3F_8 or a reactive collision of CF_3 radicals or CF_4 and CF_2 either in the gas-phase or on a surface. The identification of C_2F_6 in the infrared spectra is complicated by overlying bands of CF_2 and CF_3. Hexafluoroethane has three strong fundamental bands visible in the infrared, located at 1251, 1117, and 714 cm^{-1}.[29] The fundamentals, their assignments, and integrated absorbance cross-sections are listed in Table IV.[6,25] The calculated cross-sections are within 2 to 4% of those calculated in other works.[6] CF_2 has three vibrational modes that are active in the infrared spectrum. Past research has located the symmetric stretch band with a band head at either 1222 or 1225 cm^{-1}. The stronger absorbing asymmetric stretch band is reported[30–32] at 1102, 1112, or 1115 cm^{-1}, while a much weaker bending vibration appears[33] at 668 cm^{-1}. The strongest absorption for CF_3 is a CF stretch band reported[34–36] at both 1251 cm^{-1} and 1260 cm^{-1}. A second moderate strength stretch band is observed[37,38] between 1086 and 1089 cm^{-1}, and a much weaker umbrella vibration absorbs[37,38] between 701 and 703 cm^{-1}. There is no stable form of these free radicals. Consequently, different parent molecules and temperatures were used to create the CF_2 and CF_3 radicals. The combination of the infrared absorption of other byproducts and large temperature shifts can account for the difference in band assignments. The overlapping nature of CF_2, CF_3, and C_2F_6 absorption bands can make it very difficult to identify and accurately measure species densities. Processing plasmas traditionally using fluorocarbon feed gases exacerbate this problem because of the relatively low pressures (10–50 mTorr) and unknown radical temperatures. The low pressures and infrared radiation from the source decrease the signal-to-noise ratio, making it difficult to use weak bands for identification. Thus, it becomes imperative to have some knowledge of the radical temperature and corresponding band profiles in order to accurately distinguish between the species.

TABLE III. Band assignments and integrated absorption cross-sections for C_3F_8 taken at room temperature. Integrated cross-sections were also taken for 200 °C. These values were within 5% of those listed here. Bands at 1211 cm^{-1} and 1179 cm^{-1} were combined for the cross-section provided.

	Band (cm^{-1})	Assignment[27]	Range (cm^{-1})	Integrated Absorbance Cross-Section (cm/molecule)
A	1350.4	CF_3 Asym Stretch	1329–1391	1.5×10^{-17}
B	1297.9	CF_3 Asym Stretch	1287–1329	2.0×10^{-18}
C	1262	CF_3 Asym Stretch	1227–1287	1.40×10^{-16}
D	1209.6	CF_3 Sym Stretch	1171–1227	2.55×10^{-17}
E	1154.7	CF_2 Sym Stretch	1108–1171	2.94×10^{-17}
F	1007.1	CC Asym Stretch	959–1063	3.68×10^{-17}
G	730.9	CF_3 Asym Deform	708–754	8.37×10^{-18}

TABLE IV. Band assignments and integrated absorption cross-sections for C_2F_6 taken at room temperature. Integrated cross-sections were also taken for 200 °C. These values were within 5% of those listed here.

	Band (cm^{-1})	Assignment		Integrated Absorbance Cross-Section (cm/molecule)
A	1250	CF_3 Asym Stretch	1220–1280	1.70×10^{-16}
B	1117	CF_3 Sym Stretch	1060–1165	4.78×10^{-17}
C	714	CF_3 Sym Deform	680–760	6.12×10^{-18}

The peak of the asymmetric stretching band of C_2F_6 (Fig. 7) can be used to estimate the temperature of the species.

$$T = (-1.469\upsilon_{\max} + 1853.2)^2. \quad (12)$$

The standard deviation of the residual and the resolution error create a minimum error of ±22 K. As can be seen in Fig. 8, the Q branch of the symmetric stretching band at 1117 cm^{-1} decreases significantly as temperature increases. However, the shift of the branch maximum is not sufficient to estimate the temperature with a meaningful error. More work is needed to demonstrate the band profile changes of CF_2 and CF_3 radicals with increasing temperature.

E. C_2F_4

Tetrafluoroethylene (C_2F_4), while mainly used in the production of polytetrafluoroethylene,[39] is a product in many fluorocarbon plasmas.[40] In addition, it is being investigated as a possible alternative to saturated perfluoro-compounds in plasma etching systems.[39] Tetrafluoroethylene has two strongly absorbing fundamental bands in the infrared spectrum. The asymmetric and symmetric CF_2 stretch vibrations absorb at 1337 and 1186 cm^{-1}, respectively (Fig. 9).[29] The integrated absorbance cross-sections, tabulated in Table V, are within 0.3% of the cross-sections presented by Drage *et al.*[41] Both bands can be easily obscured by significant amounts of C_3F_6, C_3F_8, or *c*-C_4F_8. However, a set of isolated combination bands at 3208 and 3058 cm^{-1} can also be used to identify the presence of C_2F_4 if there is sufficient SNR. As seen in Figs. 2 and 3, the only other fluorocarbon absorption in this range is from C_3F_6.

Temperature can be determined from the R branch of the asymmetric stretch band (1337 cm^{-1}). However, because of the large amount of absorption from other species, accurate temperature analysis can only be undertaken after other species have been removed from the spectrum. Eq. (13) describes how the location of the R branch maximum can be used to obtain the temperature of the species.

$$T = (-1.444\upsilon_{\max} + 1939.7)^2. \quad (13)$$

The standard deviation of the residual and the instrument error give an uncertainty of ±11 K

F. CF_4

The infrared absorbance spectrum of tetrafluoromethane (CF_4) has been the subject of numerous studies due to its potency as a greenhouse gas and its prevalence in manufacturing as a low-temperature refrigerant and plasma etchant. Despite the abundant research devoted to the infrared spectra, results for the integrated absorbance cross-section of CF_4 vary by up to 50%.[7,25,42–48] In contrast, for the other gases presented in this article, the reported absorbance cross-sections rarely vary more than 5% among authors. Five percent variation is expected due to a combination of instrument and measurement errors. Little explanation has been provided for the unexpected range of values in literature for CF_4. One recent paper suggests that some of the researchers underestimate the cross-section of the υ_3 absorption band because of saturation of the Q branch.[49] The aberrations on the other side of the data were explained as an underestimation of the CF_4 concentration in the gas mixture. In order to resolve the experimental

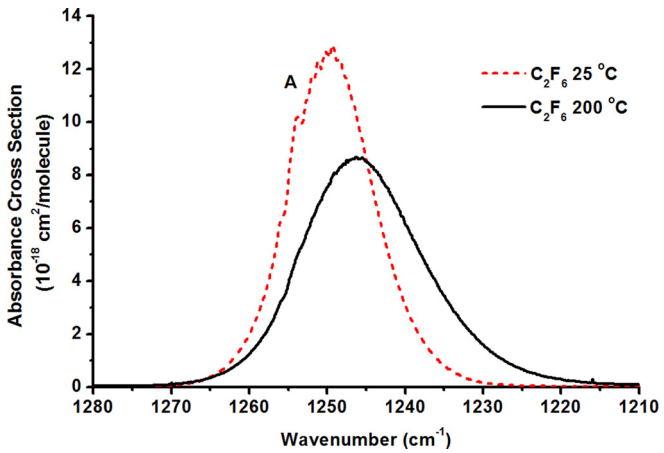

FIG. 7. (Color online) Absorbance cross-section of C_2F_6 CF_3 Asymmetric stretch band from 1210 to 1280 cm^{-1} for 25 and 200 °C gas temperatures. Capital letter band structure designations can be found in Table IV.

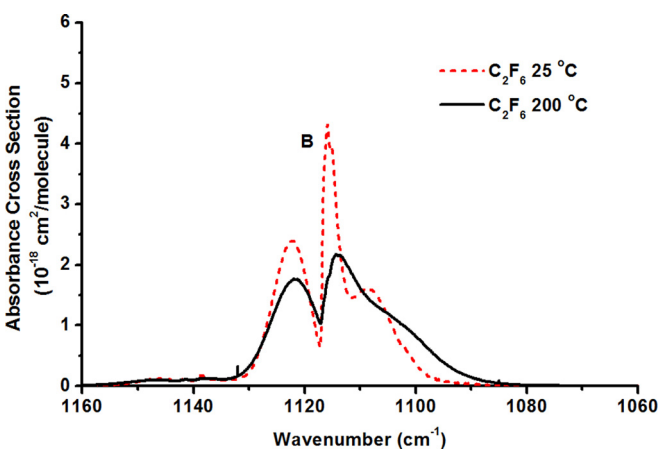

FIG. 8. (Color online) Absorbance cross-section of C_2F_6 CF_3 Symmetric stretch band from 1060 to 1160 cm^{-1} for 25 and 200 °C gas temperatures. Capital letter band structure designations can be found in Table IV.

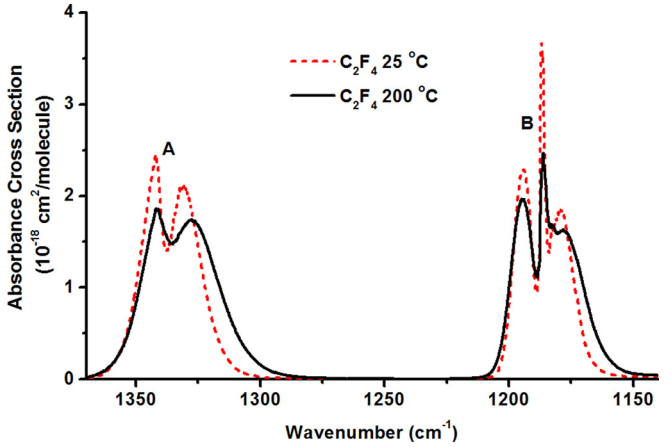

FIG. 9. (Color online) Absorbance cross-sections of C_2F_4 from 1025 to 1375 cm^{-1} for 25 and 200 °C gas temperatures. Capital letter band structure designations can be found in Table V.

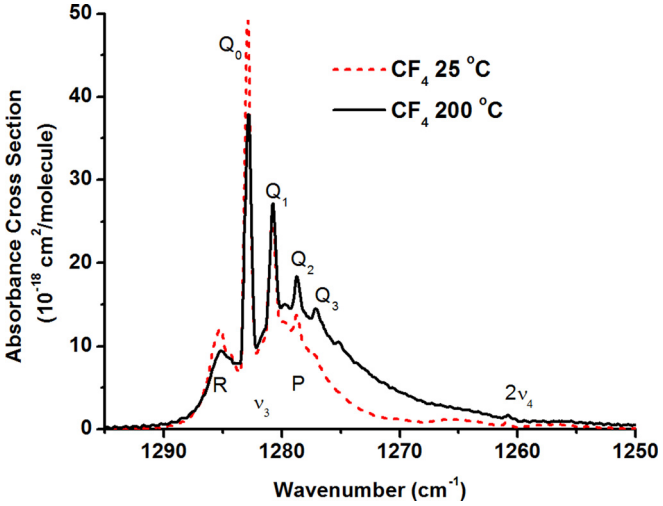

FIG. 10. (Color online) Absorbance cross-section of CF_4 CF stretch band from 1250 to 1300 cm^{-1} for 25 and 200 °C gas temperatures (2 mTorr and 325 cm path length).

differences, CF_4 absorption measurements were taken under a variety of circumstances. The measurements were performed for a range of pressures, CF_4 concentrations, wall temperatures, and path lengths. The results support an aberration from the linear absorption regime of Beer's law under most of the experimental conditions.

Although CF_4 has four fundamental vibration transitions υ_1, υ_2, υ_3 and υ_4, located at 908.5 cm^{-1}, 435 cm^{-1}, 1283.2 cm^{-1}, and 635 cm^{-1}, respectively, only the υ_3 transition is active in the IR region available to the MCT A detector used in the present study. Figure 10 shows the absorption of the υ_3 and the $2\upsilon_4$ transitions for 25 and 200 °C gas temperatures, taken at 2 mTorr with a 325 cm path length. A number of factors complicate the absorption of this peak. The Q branch is extremely sharp, causing it to be highly affected by pressure broadening, as well as prone to saturation for the pressures and path lengths commonly used in plasmas. In addition, the Q branch is perturbed by both Fermi resonance and a possible Coriolis interaction[50] with the $2\upsilon_4$ and $3\upsilon_2$ overtones. Finally, strong hot bands appear superimposed over the P branch arising from $\upsilon_3+n\upsilon_2-n\upsilon_2$ transitions.[50] While these characteristics serve to make this structure immediately recognizable in almost any concentration, they complicate the calculation of absolute density measurements taken from the integrated absorption intensity.

Figures 11 and 12 show the integrated absorbance for the Q branches and the entire υ_3 transition as a function of the density and path length ($n*l$). A υ_3 cross-section of 2.29×10^{-16} cm/molecule loosely fits the lowest densities and pathlengths. This cross-section is in agreement with the largest cross-sections found in literature. As the product of density and path length increases, the cross-section monotonically decreases, allowing for the range of values found by other researchers. A clear dependence on $n*l$ is consistent with saturation of the IR signal. However, nonlinearity appears well before the Q branch begins to absorb more than 80% (the absorbance where other species begin to show nonlinear saturation effects) of the signal. Other authors have attributed the early onset of this nonlinearity to the sharpness of the Q branch coupled with resolution limititations.[10] However, Fig. 12 also shows the difference between the υ_3 and the Q_0 and Q_1 branches, which display the same nonlinearity. In addition, the shape of the absorption cross-section is shifted with the $n*l$ product. This effect is shown in Fig. 13 as the cross-section changes for all of the branches of the υ_3 transition even when the transmittance exceeds 80%. Figure 13 also shows the shape of the R branch shifting as a function of the product of density and pathlength.

These combined observations indicate that the linear version of Beer's law cannot be applied under conditions useful for absolute density measurements in processing plasmas. The results also cast doubt on the validity of the translational temperature measurement of CF_4 based on the relative absorbance of the hot bands. Further work is needed at a higher resolution to examine the source of the nonlinearity. In order to obtain absolute density measurements of CF_4, the authors have taken a wide range of measurements as a function of the gas temperature and the density and path length product. After measuring the temperature of other gases in the system, the absorbance profile can be fitted to one of these measurements, providing a density with relavent error bars.

TABLE V. Band assignments and integrated absorption cross-sections for C_2F_4 taken at room temperature. Integrated cross-sections were also taken for 200 °C. These values were within 5% of those listed here.

	Band (cm^{-1})	Assignment	Range (cm^{-1})	Integrated Absorbance Cross-Section (cm/molecule)
A	1337	CF_2 Asym Stretch	1250–1400	6.20×10^{-17}
B	1186	CF_2 Sym Stretch	1150–1220	5.52×10^{-17}

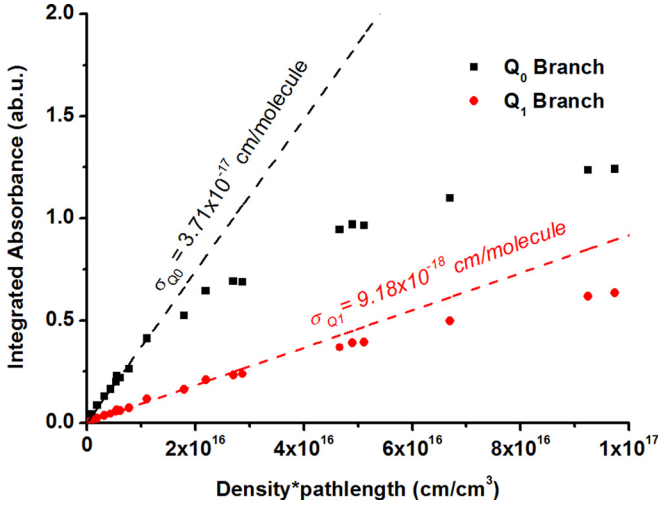

FIG. 11. (Color online) CF_4 Q Branch integrated absorption at 25 °C vs the density and pathlength product.

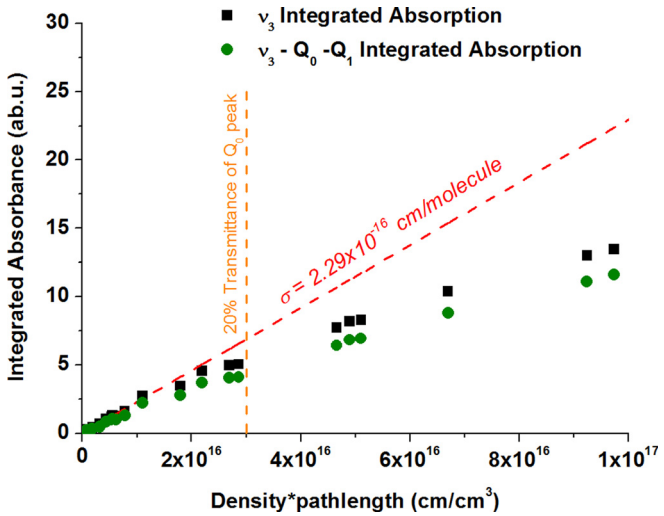

FIG. 12. (Color online) CF_4 υ_3 integrated absorption as a function of the product of density and pathlength at 25 °C.

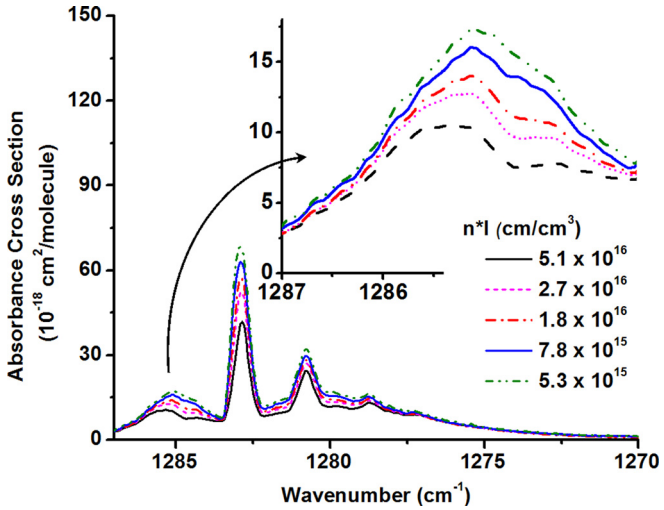

FIG. 13. (Color online) Change in absorbance cross-section of CF_4 from 1250 to 1300 cm−1 taken at 25 °C for a range of densities and pathlengths.

VI. CONCLUSION

The infrared spectra for the most common stable species present in fluorocarbon plasma systems have been presented. A method for identifying species, as well as determining densities and temperatures within appropriate error limits has been presented. These results have been limited to a maximum temperature of 200 °C in a temperature-averaged system. The results have shown that in this temperature range (for all species except CF_4) there are significant changes in the absorption profiles, but only trivial changes in the integrated absorbance cross-sections of the various vibrational-rotational bands. Further work is needed to expand the temperature range of these species, as well as explore the temperature variation of the infrared absorption of free radical species such as CF, CF_2, and CF_3.

ACKNOWLEDGMENT

This work was supported in part by a gift from Applied Materials.

[1]B. Smith, *Fundamentals of Fourier Transform Infrared Spectroscopy*, (CCP, FL, 1996).
[2]L. A. Farrow, J. Chem. Phys. **82**, 3625 (1985).
[3]J. C. Knights, J. P. M. Schmitt, J. Perrin, and G. Guelachvili, J. Appl. Phys **76**, 3414 (1982).
[4]T. A. Cleland and D. W. Hess, J. Appl. Phys. **64**, 1068 (1988).
[5]L. N. Ignat'eva and V. M. Buznik, Russ. J. Phys. Chem. **80**, 1940 (2006).
[6]Q. Zou, C. Sun, V. Nemtchinov, and P. Varanasi, J. Quant. Spectrosc. Radiat. Transf. **83**, 215 (2004).
[7]V. Nemtchinov and P. Varanasi, J. Quant. Spectrosc. Radiat. Transf. **82**, 461 (2003).
[8]M. Haverlag, F. J. de Hoog, and G. M. W. Kroeson, J. Vac. Sci. Technol. A **9**, 327 (1991).
[9]M. J. Goeckner, M. A. Henderson, J. A. Meyer, and R. A. Breun, J. Vac. Sci. Technol A **12**, 3120 (1994).
[10]B. A. Cruden, M. V. V. S. Rao, S. P. Sharma, and M. Meyyappan, Plasma Sources Sci. Technol. **11**, 77 (2002).
[11]B. Zhou, E. A. Joseph, S. P. Sant, Y. Liu, A. Radhakrishnan, L. J. Overzet, and M. J. Goeckner, J. Vac. Sci. Technol. A **23**, 1657 (2005).
[12]S. P. Sant, C. T. Nelson, L. J. Overzet, and M. J. Goeckner, J. Vac Sci. Technol. A **27**, 631 (2009).
[13]K. Takahashi, A. Itoh, T. Nakamura, and K. Tachibana, Thin Solid Films **374**, 303 (2000).
[14]K. Takahashi and K. Tachibana, J. Vac. Sci. Technol. A **20**, 305 (2002).
[15]M. J. Goeckner, J. M. Marquis, B. J. Markham, A. K. Jindal, E. A. Joseph, and B. Zhou, Rev. Sci. Instrum. **75**, 884 (2004).
[16]J. D. J. Ingle and S. R. Crouch, *Spectrochemical Analysis* (Prentice Hall, NJ, 1988).
[17]H. P. Knauss and M. S. McCay, Phys. Rev. **52**, 1143 (1937).
[18]M. M. Smit-Miessen and J. L. Spier, Physica **9**, 193 (1942).
[19]J. L. Spier and J. A. Smit, Physica **9**, 597 (1942).
[20]G. Herzberg, *Molecular Spectra and Molecular Structure* (D. Van Nostrand Company, Inc, Canada, 1950).
[21]G. D. Fischer, R. L. Purchase, and D. M. Smith, J. Mol. Struct. **145**, 159 (1997).
[22]R. P. Bauman and B. J. Bulkin, J. Chem. Phys. **45**, 496 (1966).
[23]J. Ballard, R. J. Knight, and D. A. Newnham, J. Quant. Spectrosc. Radiat. Transf. **66**, 199 (2000).
[24]J. Cl. Leicknam, M. Campos-Vallette, and M. Rey-Lafon, Mol. Phys. **43**, 983 (1982).
[25]C. M. Roehl, D. Boglu, C. Bruhl, and G. K. Moortgat, Geophys. Res. Lett. **22**, 815 (1995).
[26]T. Masuoka, T. Iwatsubo, and K. Mizoguchi, J. Membr. Sci. **69**, 109 (1992).
[27]E. L. Pace, A. C. Plaush, and H. V. Samuelson, Spectrochim. Acta **22**, 993 (1966).

[28]J. Feldsien, D. Kim, and D. J. Economou, Thin Solid Films **374**, 311 (2000).
[29]T. Shimanouchi, *Tables of Molecular Vibrational Frequencies Consolidated* (National Bureau of Standards, U.S. Govt. Print. Off., 1972), Vol. I, pp. 1-160.
[30]D. E. Milligan and M. E. Jacox, J. Chem. Phys. **48**, 2265 (1968).
[31]A. S. Lefohn and G. C. Pimentel, J. Chem. Phys. **55**, 1213 (1971).
[32]K. C. Herr and G. C. Pimentel, Appl. Opt. **4**, 25 (1965).
[33]V. E. Bondybev, J. Mol. Spectrosc. **63**, 164 (1976).
[34]J. Newton and W. Person, J. Chem. Phys. **68**, 2799 (1978).
[35]C. Yamada and E. Hirota, J. Chem. Phys. **78**, 1703 (1983).
[36]G. Carlson and G. A. Pimentel, J. Chem. Phys. **44**, 4053 (1966).
[37]D. Forney, M. E. Jacox, and K. K. Irukura, J. Chem. Phys. **101**, 8290 (1994).
[38]M. Suto and N. Washida, J. Chem. Phys. **78**, 1012 (1983).
[39]G. Acerboni, N. R. Jensen, B. Rindone, and J. Hjorth, Chem. Phys. Lett. **309**, 364 (1999).
[40]V. M. Donnelly and D. L. Flamm, Solid State Technol. **24**, 161 (1981).
[41]E. A. Drage, D. Jaksch, K. M. Smith, R. A. McPheat, E. Vasekova, and N. J. Mason, J. Quant. Spectrosc. Radiat. Transf. **98**, 44 (2006).
[42]A. H. McDaniel, C. A. Cantrell, J. A. Davidson, R. E. Shetter, and J. G. Calvert, J. Atmos. Chem. **12**, 211 (1991).
[43]P. N. Schatz and D. F. Hornig, J. Chem. Phys. **21**, 1516 (1953).
[44]B. Schurin, J. Chem. Phys. **30**, 1 (1959).
[45]I. W. Levin and T. P. Lewis, J. Chem. Phys. **52**, 1608 (1970).
[46]S. Saeki, M. Mizuno, and S. Kondo, Spectrochim. Acta. **A32**, 403 (1976).
[47]W. G. Golden, C. Marcott, and J. Overend., J. Chem. Phys. **52**, 2081 (1978).
[48]P. Varanasi and S. Chudamani, J. Geophys. Res. **93**, 1666 (1988).
[49]M. D. Hurley, T. J. Wallington, G. A. Buchanan, L. K. Gohar, G. Marston, and K. P. Shine, J. Geophys. Res. **110**, 2101 (2005).
[50]L. H. Jones, C. Kennedy, and S. Ekberg, J. Chem. Phys. **69**, 833 (1978).